Spectrochimica Acta Part B 139 (2018) 75–82

Contents lists available at ScienceDirect

Spectrochimica Acta Part B

journal homepage: www.elsevier.com/locate/sab

Three dimensional characterization of laser ablation craters using high resolution X-ray computed tomography

A.H. Galmed [a,b,f,*], A. du Plessis [c], S.G. le Roux [c], E. Hartnick [c], H. Von Bergmann [d], M. Maaza [e,f]

[a] National Institute of Laser Enhanced Sciences (NILES), Cairo University, Egypt
[b] Materials Research Department (MRD), iThemba LABS-National Research Foundation (NRF), 1 Old Faure Road, P. O. Box 722, 7129 Somerset West, Western Cape, South Africa
[c] University of Stellenbosch, CT Scanner Facility, Private Bag X1, Matieland, Stellenbosch 7602, South Africa
[d] Laser Research Institute (LRI), Physics Department, University of Stellenbosch, Stellenbosch, South Africa
[e] Nano-sciences African Network (NANOAFNET), Materials Research Department, iThemba LABS-National Research Foundation of South Africa, Old Faure Road, PO Box 722, Somerset West 7129, Western Cape, South Africa
[f] UNESCO-UNISA Africa Chair in Nanosciences/Nanotechnology, College of Science, Engineering and Technology, University of South Africa, Muckleneuk ridge, PO Box 392, Pretoria, South Africa

ARTICLE INFO

Article history:
Received 19 December 2016
Received in revised form 12 July 2017
Accepted 21 November 2017
Available online 28 November 2017

Keywords:
Computed tomography (CT)
Ablation
Crater
Average Ablation Rate (AAR)

ABSTRACT

Laboratory X-ray computed tomography is an emerging technology for the 3D characterization and dimensional analysis of many types of materials. In this work we demonstrate the usefulness of this characterization method for the full three dimensional analysis of laser ablation craters, in the context of a laser induced breakdown spectroscopy setup. Laser induced breakdown spectroscopy relies on laser ablation for sampling the material of interest. We demonstrate here qualitatively (in images) and quantitatively (in terms of crater cone angles, depths, diameters and volume) laser ablation crater analysis in 3D for metal (aluminum) and rock (false gold ore). We show the effect of a Gaussian beam profile on the resulting crater geometry, as well as the first visual evidence of undercutting in the rock sample, most likely due to ejection of relatively large grains. The method holds promise for optimization of laser ablation setups especially for laser induced breakdown spectroscopy.

1. Introduction

The ability of the laser to ablate material from the surface of a sample is a very important characteristic in many industrial applications like laser welding and drilling or some spectroscopic applications like Laser Induced Breakdown Spectroscopy (LIBS) as well as many other scientific applications. The laser ablation removal rate is referred to by Average Ablation Rate (AAR) which is the amount of material removed per pulse. This was expressed either by the mass of material removed per pulse, depth created per pulse or crater volume created per pulse. This ablation rate is important as it affects the speed at which material is removed, especially important when underlying material needs to remain undamaged as in the case of rock removal from around a fossil for example [1]. It also affects the depth profile resolution of sequential analysis such as depth profiling LIBS, see for example [2]. Generally, the ablation rate should be constant for good LIBS analytical performance, for quantitative measurements of elemental composition, see for example [3] or a detailed review article [4].

Many laser parameters (wavelength, pulse energy, focusing, spot size, pulse duration and beam profile) [5–7] and sample physical parameters (optical absorption, surface reflectivity, thermal conductance, etc.) can affect the AAR [8,9]. Also asymmetric ablation or non-ideal ablation will negatively impact the resulting spectral data acquisition. This was discussed in details in the details in the work of V. Lednev et al. and W.L. Yip et al. [10,11]. Studying the AAR and the crater morphology can be done by many ways. The simplest method is when a sample in the form of a thin layer is ablated until a through-hole is generated and the number of pulses counted, as was used in a detailed study of femtosecond laser ablation for example [12]. Another popular way is by using the reflection microscope [7,13] where the crater depth and width can be measured. Another similar way is by using a metallographic microscope; in 2008 Stafe et al. [14] used the metallographic microscope to investigate the nanosecond laser ablation rate. Real time AAR crater characterization was done by Janez Diaci [15], where a characterization of craters produced in hard dental tissues by two different Erbium lasers was achieved using laser profilometry. This work was followed by the work of Mezzapesa et al. [16] were they made a real time ablation rate measurement during high aspect-ratio hole drilling with a 120 ps fiber laser.

Confocal microscopes have also been used for measuring the crater depth. In 2012 Pietroy et al. [17] measured the femtosecond laser volume ablation rate, using a confocal microscope to characterize the

* Corresponding author at: National Institute of Laser Enhanced Sciences (NILES), Cairo University, Egypt.
E-mail address: Ahmedgalmed@niles.edu.eg (A.H. Galmed).

https://doi.org/10.1016/j.sab.2017.11.011
0584-8547/

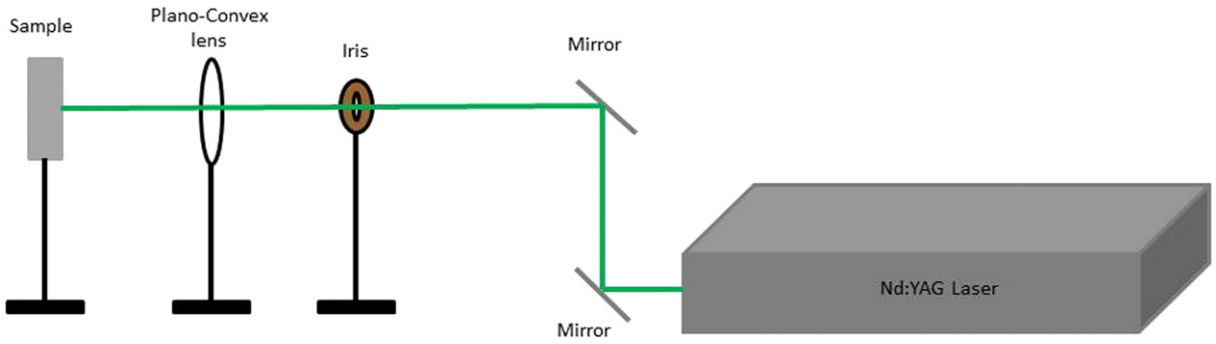

Fig. 1. Laser ablation experimental setup.

laser produced crater. Electron microscopes as well as atomic force microscopes were used by Bonse et al. [18] to study the crater morphology when they were studying femtosecond laser processing of TiN on silicon. This work was followed by the work of Sanner et al. in 2009 [19] when they measured the femtosecond laser-induced damage and ablation thresholds in dielectrics using atomic force microscopy besides the optical microscope.

Also the white light interferometer has been used in the work of J. Picard et al., where they studied the crater morphology of laser induced craters in copper at different laser energy and different pressures [20].

All the methods above rely in some form on a surface analysis, and are all limited in their ability to fully characterize the high-aspect ratio of laser ablation craters, potentially losing useful information such as undercuts for example.

X-ray micro computed tomography was first used to characterize laser ablation craters by Mercer et al. [21], where they made sequential 3D X-ray microtomographic images of enamel and dentine ablation by an Er:YAG laser. In this study they were able to visualize craters as a function of number of pulses and showed that 3D X-ray microtomography is a useful tool for quantitative measurements in dental research, though the resolution was limited to 100 μm. In subsequent work the same authors studied tooth ablation using higher resolution X-ray micro computed tomography [22]. One other study of laser ablation made use of microCT imaging of through-holes [23]. The use of X-ray micro computed tomography is increasing in various fields as shown in reviews of the technique in materials sciences [24], geosciences [25] and food sciences [26], amongst others. Some of the reasons for the increased use of this non-destructive method are its increasing accessibility [27] and the advantages of full 3D imaging which allows visualization and quantification of crater morphology and dimensions.

Though X-ray micro computed tomography has been used in some studies to image laser ablation craters and through-holes, this has been limited in scope. The potential to fully characterize the details of crater morphology has not yet been demonstrated, especially within the context of laser ablation for analytical purposes, e.g. LIBS. For analytical requirements the crater morphology is extremely important to ensure that accurate results are obtained.

In this work we investigate Nd:YAG laser induced crater morphology for two sample types typical for LIBS systems: homogeneous aluminum alloy samples and inhomogeneous rock samples. We demonstrate high resolution micro computed tomography and apply advanced analyses on the acquired data: in particular the crater volume, width, depth and cone angle were measured. The crater shape is then simulated with a theoretical model in combination with the obtained measurements. These measurements are shown to be useful for characterizing systems where laser ablation is particularly important for analytical purposes.

2. Experimental procedure

A Nd:YAG laser (Continuum NY-81, 1064 nm, 10 ns) was used to produce different craters on aluminum and rock samples. The laser was filtered spatially using a 3 mm aperture in order to obtain the best possible beam profile. The laser was then focused using a 10 cm quartz lens onto the surface of the samples under study. The focal spot diameter for the Gaussian laser beam was calculated using the equation ($d = 1.22\,\lambda f/D$), where d is the focal spot diameter, λ the laser wavelength, f the lens focal length and D the beam diameter before focusing. The samples were put 2 mm before the focus in order to prevent air

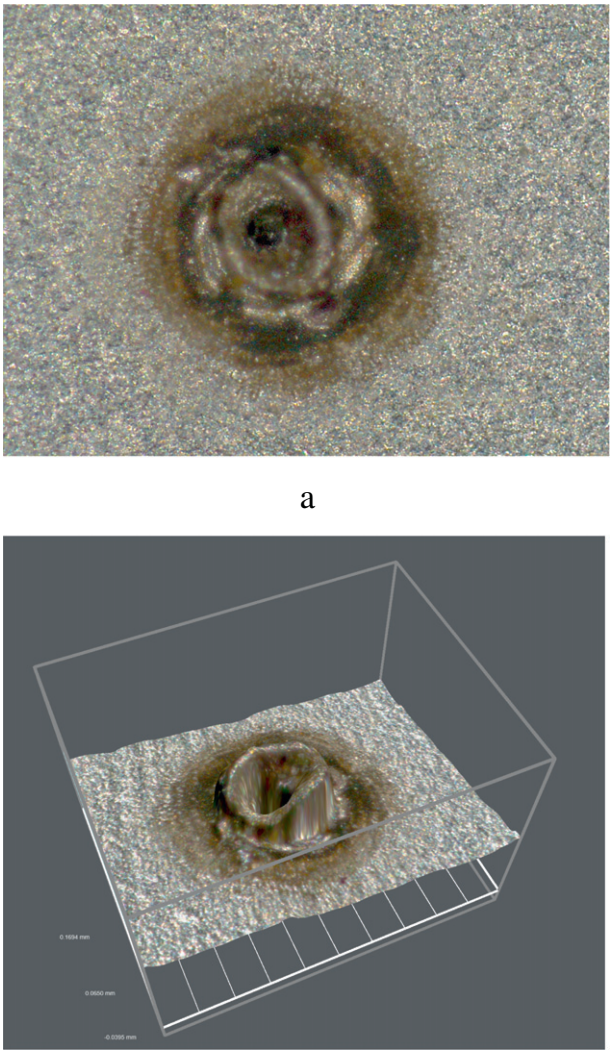

Fig. 2. 2D (a) and 3D (b) optical microscope picture taken for a 200 laser shot crater in aluminum at laser pulse energy of 51 mJ.

breakdown. This made the calculated focal spot diameter on the surface 102 μm. The craters were formed by different numbers of laser pulses delivered (50, 100, 200, 300, 400 and 500 shots) and with different laser pulse energies (12 mJ, 31 mJ, 42 mJ and 51 mJ). The sample was fixed on a translational stage so that the distance between the craters could be adjusted to prevent the overlap of two craters.

Two samples types were selected for this study, a homogeneous metal alloy and an inhomogeneous rock sample. The aluminum alloy samples were cut to dimensions (1.5 cm × 5.0 cm). Rock samples used were from Witwatersrand gold ore, containing quartz and various sulphide phases as well as microscopic gold particles. The samples were cut and polished in order to have smooth surfaces for the study. The laser at 51 mJ was used to induce craters on the rock samples with different shot numbers (50, 100, 200, 300, 400 and 500 shots). In order to overcome the inhomogeneity of the rock samples, 3 craters at different positions were done for each shot number, and then the average measurements were taken. The experimental setup is shown in Fig. 1.

X-ray micro computed tomography was carried out at the Stellenbosch CT facility [25], using a General Electric Nanotom S system. Scans were done at relatively fast scan times of approximately 30 min

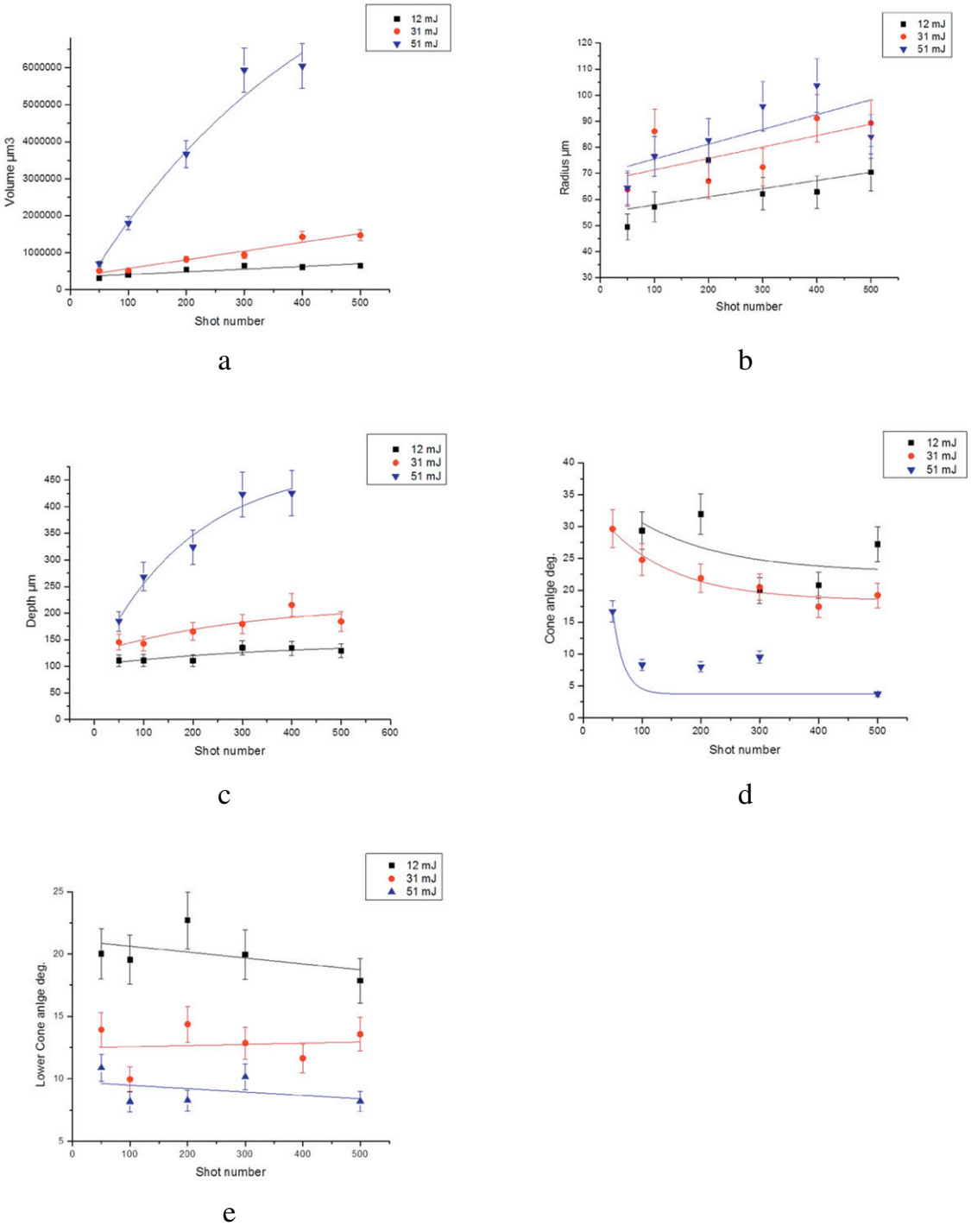

Fig. 3. Aluminum alloy crater volume (a), radius (b), width (c), cone angle (d) and lower cone angle (e) as a function of number of shots for different laser pulse energies.

per sample, using 150 kV and 100 μA and 0.5 mm copper beam filtration. Reconstructed data was analyzed in Volume Graphics VGStudioMax 3.0. Measurements of crater width, depth, volume and cone angle were made as follows. The system uses advanced surface determination software for dimensional measurements. For volume measurement, the open crater at the surface is sealed and internal volume selected as a region of interest and volume measured from this region. At the surface, the top-view is used to analyze the crater width, by fitting a 2D circle to the crater and measuring its radius. Crater depth is determined by selecting the deepest point in the crater and measuring the shortest distance between this point and the plane on the surface. Cone angles were measured in two ways: the first method used a number of fit points along the inside of the crater to fit a best-fit cone to the crater. This method was found to be biased by a large surface ablation region caused by Gaussian beam profile especially at large ablation rates. For this reason a second cone angle was measured using fit points deeper in the crater rather than near the surface. The cone angle calculation was done using the software of CT scan where the cone margins are determined and then the software calculates the cone angle. Also optical microscope images were done using Zeiss smartzoom 5 microscope.

3. Results and discussion

As mentioned in the literature [9] the crater formed by nanosecond laser usually has a heap of molten material at its opening which appears in a volcanic shape. Also some of the ablated material dust may deposit around the opening of the crater. Due to the high temperature during the ablation process a change of the metallic colour around the crater may occur in the region where the heat is transferred in the metal. All these regions can be seen in Fig. 2 which shows the optical microscope pictures taken for a 200 laser shot crater in aluminum at laser pulse energy of 51 mJ.

For a complete study of the crater morphology, the following parameters were measured from the X-ray tomography data: crater volume, width, depth and cone angle. The effects of laser pulse energy and number of shots were observed on these variables. It is expected that higher pulse energy and numbers of shots produce higher AAR. On plotting the volume change as a function of shot number for different laser pulse energy (Fig. 3a) it was observed that the volume increases with increasing shot number as expected. On increasing the laser pulse energy this increase has a faster regime. While the data is relatively limited, it seems that for a laser pulse energy of 51 mJ, the volume increase reaches a certain plateau. The Average Ablation Rate for volume (AAR_v) was found to be between 18,300 μm^3/shot for the laser pulse energy 51 mJ and 2730 μm^3/shot for the laser pulse energy 12 mJ.

When plotting the measured surface crater radius change as a function of shot numbers and laser pulse energy (Fig. 3b) it was found that both also increase linearly with increasing shot number. In the case of crater depth (Fig. 3c) it was found that the crater depth increased exponentially with laser shot number until reaching a plateau. This behavior becomes more obvious with higher laser pulse energy.

Due to the Gaussian distribution of the of the laser energy on the laser spot, the crater will not have a perfect cone shape due to the difference in the ablation rate in the margins of the crater than that in the center. This will make conical shape of the crater to have a wider angle near the surface than in the center. That is why the crater cone angle measurements were done by the two methods described in the previous section, with the second method giving a better representation of the crater internal cone, rather than the surface ablation around the top crater edge (Fig.4).

On measuring the first cone angle from the top of the crater to the bottom (Fig. 3d), it was found that as the number of shots increases the cone angle decreases exponentially. It can also be observed that the crater induced by lowest laser pulse energy of 12 mJ shows the largest cone angles which then decreases with increasing energy.

This case was different on measuring the cone angle for the lower part of the cone only (Fig. 3e). Here the cone angle is almost constant or varies only slightly. Also it was found that with increasing pulse energy the cone angle increases.

The previous results can be attributed to the fact that as the laser fluence increases the amount of the ablated mass (m) increases following the equation [9]:

$$m = E(1-R)/\left[C_p(T_b - T_0) + L_v\right] \quad (1)$$

where (E) is the laser pulse energy, (R) the surface reflectivity, (C_p) specific heat, (T_b) the boiling point (K), (T_0) the room temperature (K), and (L_v) the latent heat of vaporization. This expression can be converted to ablated depth per pulse by using fluence (F) instead of (E), and dividing by the density of the material.

Also as the number of shots increases the amount of ablated mass increases, leading to an increase in the volume as well as the depth [9]. Since the central part of the laser beam is much more intense than the margins the crater radius at the top increasing with a slower rate than

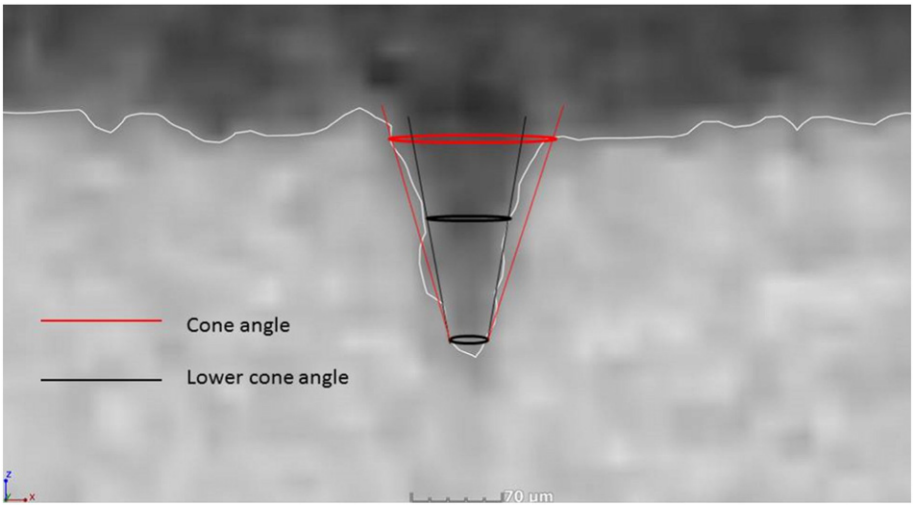

Fig. 4. Cone angles measuring for the craters.

that of the central part which in turns leads to a decrease the cone angle of the crater. This was confirmed by the angle measurement of the lower part of the cone where the laser fluence is higher, resulting in an almost constant or slowly varying angle; since the outer part of the cone is excluded. This is confirmed by the later simulation.

On repeating the experiment for the rock samples using the laser pulse energy 51 mJ it was found that the results show similar trends (Fig. 5). Fig. 5a shows an increase of the induced crater volume with increasing number of laser shots. However, the values for the crater volume are much lower than that of the aluminum sample for the same laser pulse energy.

Similarly, the crater radius increases linearly with the laser shot number (Fig. 5b), although the increase is smaller than for the aluminum samples. The crater depth (Fig. 5c) shows the same behavior, also increasing linearly with the number of laser shots but with lower values than for aluminum.

Again this can be attributed to the fact that the amount of ablated mass increases with shot number [9]. Also as it was observed that the values in case of rock samples are much lower than for aluminum samples. This is due to the difference in amount of ablated mass as a function of laser fluence and ablation threshold of the rock samples compared to those of aluminum as indicated by Eq. (1) [9].

On studying the change of the cone angle as a function of laser shot number it was found to be decreasing exponentially with the laser shot number both in case of the cone angle measured from top to bottom or for the lower part of the cone only (Fig. 5d, e). Here the similarity of the

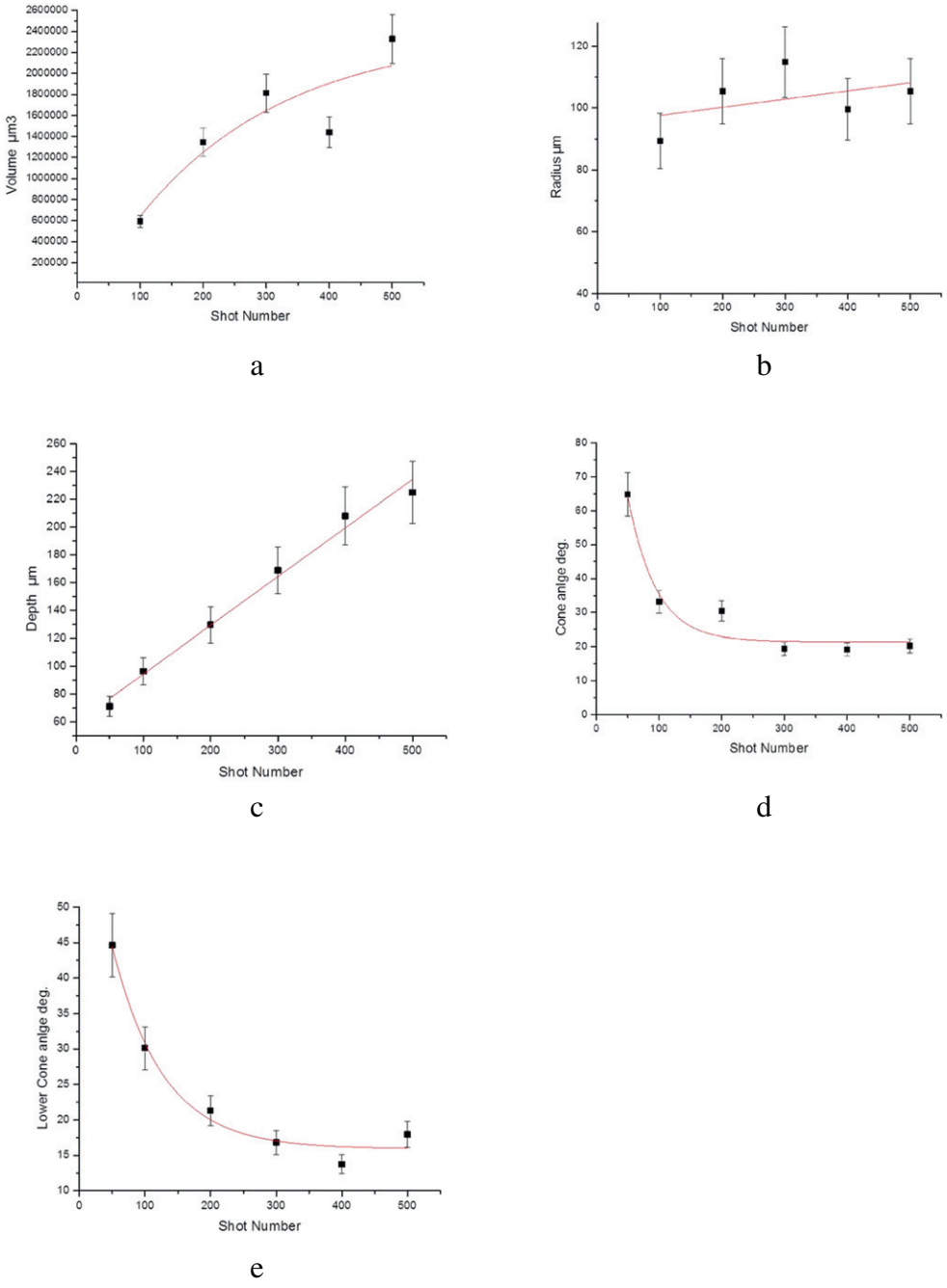

Fig. 5. Rock crater volume (a), radius (b), width (c), cone angle (d) and lower cone angle (e) as a function of number of shots.

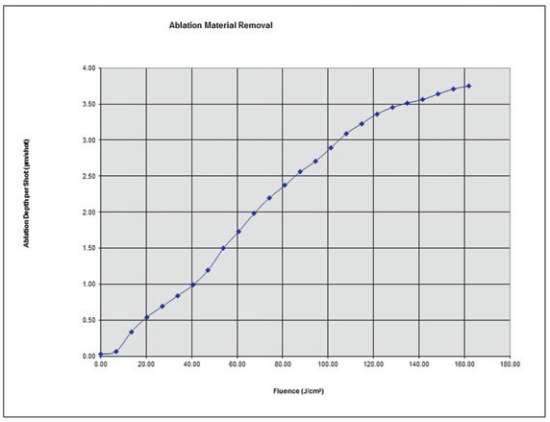

a

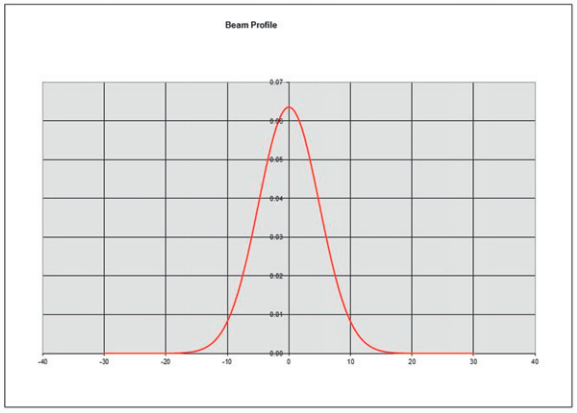

b

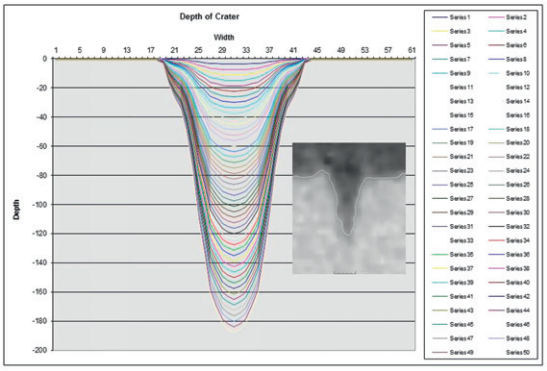

c

Fig. 6. Crater simulation results: estimated ablated depth per shot vs. laser fluence (a), the laser Gaussian beam profile (b), simulated crater (c).

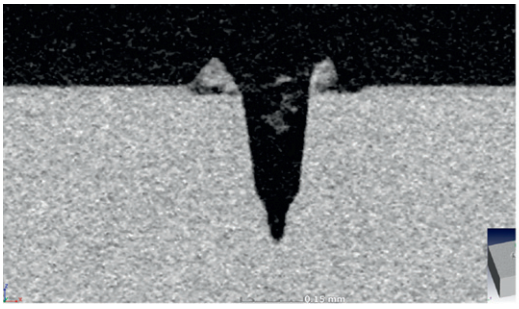

a

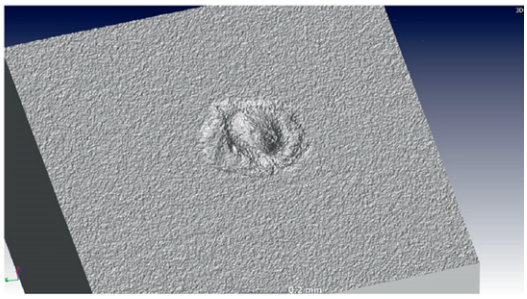

b

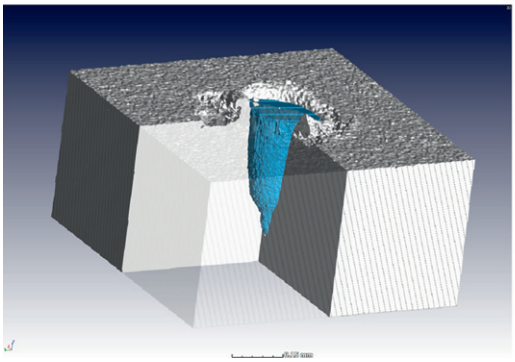

c

Fig. 7. High resolution images for a 200 laser shot crater in aluminum at laser pulse energy of 51 mJ: 2D crater (a), 3D crater top (b).

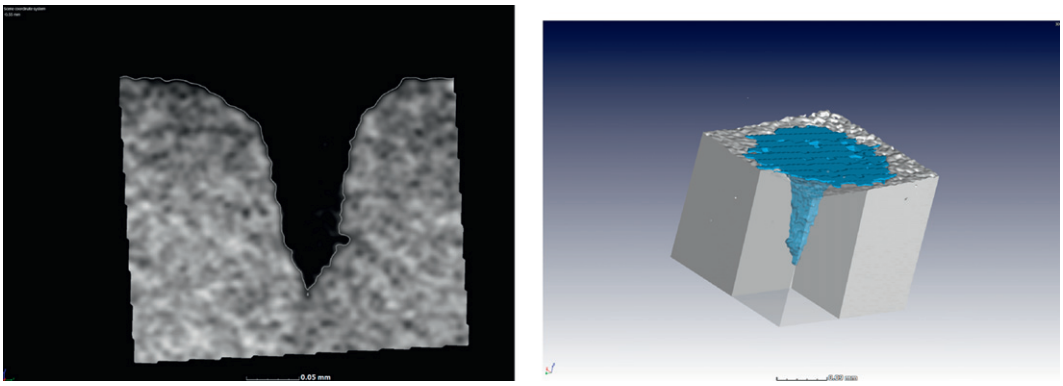

Fig. 8. High resolution images for a 400 laser shot crater in rock sample at laser pulse energy of 51 mJ: 2D crater (a), 3D crater (b).

behavior of both cone angles is an indicator for the low amount of material ablated at the margins due to the more difficult ablation of the rock compared to aluminum [9].

In order to get a better understanding of the obtained results, a theoretical simulation was carried out to estimate the dependence of the crater shape on the ablated mass as function of laser intensity and beam profile [7]. The simulation was done for the crater induced by 50 laser shots in the Al sample.

In this simulated model the laser spot area was divided into (61 × 61) squares then the pulse intensity was distributed on the beam area according to the beam profile assumed in the simulation. Gaussian beam profile is used in this study. The ablated depth per pulse as a function of laser fluence was then fed into the simulation in order to get the best shape of the crater that is similar to the experimental one. Here the simulation simulates the ablation that is done after each laser pulse and the overall crater shape is estimated after 50 laser shots.

The best suggested ablated depth-fluence regime in order to simulate the actual experimental results was found to be the exponential increase of ablated mass as function of laser fluence as can be seen in Fig. 6a, which was found to be in a good agreement with the work of Vladoiu et al. [28,29] except for the values of the depth per pulse since the samples used in our work is a harder Al alloy samples not pure Al. Using the Gaussian beam profile shown in Fig. 6b, the crater derived from the simulation is shown in Fig. 6c which closely resembles the experimental crater shape.

This simulation didn't work with the rock samples since the samples are not homogenous and so they don't have a fixed ablated depth-fluence regime. But this was also an indication that the estimated one for Al was a good one.

In order to test the ability of the CT scan to obtain more information about the crater, a high resolution scan was made for the crater induced by 200 laser shots with 51 mJ pulse energy (Fig. 7). Fig. 7a shows the 2D high resolution scan of the crater. As can be seen the crater shape is obviously conical and the cone angle for the bottom part is smaller than that of the upper part. Also the residual ablated material that is thrown out of the crater can be seen at the upper part of the crater. This residue can also be observed more clearly in the 3D image of the upper part of the crater (Fig. 7b). Also the complete 3D crater shape can be seen in Fig. 7c. This is in a very good agreement with craters induced by nanosecond lasers reported in previous work [30,31].

The CT scan was also able to detect much more details in the rock samples. Fig. 8 shows the high resolution scan for a hole in the rock sample generated by 400 laser shots of 51 mJ pulse energy. As can be seen in the 2D crater image of Fig. 8a there is a small side hole near the bottom of the crater. This hole can be seen again in the 3D image (Fig. 8b). This hole is suggested to be due to the ablation of a small granule at the side of the crater due to the high temperature of the plasma. This may affect the plasma emission spectrum due to a sudden introduction of this granule into the plasma. Fig. 8 indicates the ability of the CT scan to see the undercut of the laser induced craters and monitor any sudden change in the spectrum observed from the plasma emission.

4. Conclusion

From the results reported in this work it can be concluded that the CT scan serves as an extremely useful technique for examining the shape of laser ablation induced craters. The CT scan enables the accurate measurement of the crater volume, width, depth and cone angle, closely resembling results obtained from the theoretical simulation model. Also through very high resolution undercut images of the crater it can reveal very fine details that can't be seen by other crater investigation methods. These details can be very useful for some spectroscopic investigations.

References

[1] D.E. Roberts, A. Du Plessis, J. Steyn, L.R. Botha, S. Pityana, L.R. Berger, "An investigation of Laser Induced Breakdown Spectroscopy for use as a control in the laser removal of rock from fossils found at the Malapa hominin site", South Africa, Spectrochim. Acta B 73 (2012) 48–54.
[2] D.E. Roberts, A. Du Plessis, J. Steyn, L.R. Botha, C.A. Strydom, I.J. Van Rooyen, Femtosecond laser induced breakdown spectroscopy of silver within surrogate high temperature gas reactor fuel coated particles, Spectrochim. Acta B 65 (2010) 918–926.
[3] K.N. Mekonnen, A.A. Ambushe, B.S. Chandravanshi, M.R. Abshiro, A. du Plessis, R.I. McCrindle, Assessment of the concentration of Cr, Mn and Fe in sediment using laser-induced breakdown spectroscopy, Bull. Chem. Soc. Ethiop. 27 (2013) 1–13.
[4] R.S. Harmon, R.E. Russo, R.R. Hark, Applications of laser-induced breakdown spectroscopy for geochemical and environmental analysis: a comprehensive review, Spectrochim. Acta B 87 (2013) 11–26.
[5] R. Le Harzic, D. Breitling, M. Weikert, S. Sommer, C. Föhl, S. Valette, C. Donnet, E. Audouard, F. Dausinger, Pulse width and energy influence on laser micromachining of metals in a range of 100 fs to 5 ps, Appl. Surf. Sci. 249 (2005) 322–331.
[6] J.P. Desbiens, P. Masson, ArF excimer laser micromachining of pyrex, SiC and PZT for rapid prototyping of MEMS components, Sens. Actuators A Phys. 136 (2007) 554–563.
[7] A.H. Galmed, A.K. Kassem, H. Von Bergmann, M.A. Harith, A study of using femtosecond LIBS in analyzing metallic thin film–semiconductor interface, Appl. Phys. B Lasers Opt. 102 (2011) 197–204.
[8] L. Moenke-Blankenburg, Laser Micro Analysis, John Wiley & Sons, Inc., New York, 1989.
[9] David A. Cremers, Leon J. Radziemski, Handbook of Laser-Induced Breakdown Spectroscopy, John Wiley & Sons, Ltd, England, 2013.
[10] V. Lednev, S.M. Pershin, A.F. Bunkin, Laser beam profile influence on LIBS analytical capabilities: single vs. multimode beam, J. Anal. At. Spectrom. 25 (2010) 1745.
[11] W.L. Yip, N.H. Cheung, Analysis of aluminum alloys by resonance-enhanced laser induced breakdown spectroscopy: how the beam profile of the ablation laser and the energy of the dye laser affect analytical performance, Spectrochim. Acta B 64 (2009) 315–322.
[12] D.E. Roberts, A. Du Plessis, L.R. Botha, Femtosecond laser ablation of silver foil with single and double pulses, Appl. Surf. Sci. 256 (2010) 1784–1792.
[13] G. Raciukaitis, M. Brikas, P. Gecys, M. Gedvilas, Accumulation effects in laser ablation of metals with high-repetition-rate lasers, Proc. SPIE 7005 (2008) 1–11.

[14] M. Stafe, I. Vlădoiu, C. Neguþu, I.M. Popescu, Experimental investigation of the nanosecond laser ablation rate of aluminum, Rom. Rep. Phys. 60 (2008) 789–796.
[15] J. Diaci, Laser profilometry for the characterization of craters produced in hard dental tissues by Er:YAG and Er,Cr:YSGG lasers, J. Laser Health Acad. 2008 (2008) 1–10.
[16] F.P. Mezzapesa, T. Sibillano, F. Di Niso, A. Ancona, P.M. Lugarà, M. Dabbicco, G. Scamarcio, Real time ablation rate measurement during high aspect-ratio hole drilling with a 120-ps fiber laser, Opt. Express 20 (2012) 663–671.
[17] D. Pietroy, Y. Di Maio, B. Moine, E. Baubeau, E. Audouard, Femtosecond laser volume ablation rate and threshold measurements by differential weighing, Opt. Express 20 (2012) 29900–29908.
[18] J. Bonse, M. Geuss, S. Baudach, H. Sturm, W. Kautek, The precision of the femtosecond-pulse laser ablation of TiN films on silicon, Appl. Phys. A Mater. Sci. Process. 69 (1999) S399–S402.
[19] N. Sanner, O. Utéza, B. Bussiere, G. Coustillier, A. Leray, T. Itina, M. Sentis, Measurement of femtosecond laser-induced damage and ablation thresholds in dielectrics, Appl. Phys. A Mater. Sci. Process. 94 (2009) 889–897.
[20] J. Picard, J.-B. Sirven, J.-L. Lacour, O. Musset, D. Cardona, J.-C. Hubinois, P. Mauchien, Characterization of laser ablation of copper in the irradiance regime of laser-induced breakdown spectroscopy analysis, Spectrochim. Acta B 101 (2014) 164–170.
[21] C.E. Mercer, P. Anderson, G.R. Davis, Sequential 3D X-ray microtomographic measurement of enamel and dentine ablation by an Er:YAG laser, Br. Dent. J. 194 (2003) 99–104.
[22] J. Fearne, P. Anderson, G.R. Davis, 3D X-ray microscopic study of the extent of variations in enamel density in first permanent molars with idiopathic enamel hypomineralisation, Br. Dent. J. 196 (2004) 634–638.
[23] H.C. Wang, H.Y. Zheng, P.L. Chu, J.L. Tan, K.M. Teh, T. Liu, B.C.Y. Ang, G.H. Tay, Femtosecond laser drilling of alumina ceramic substrates, Appl. Phys. A Mater. Sci. Process. 101 (2010) 271–278.
[24] E. Maire, P.J. Withers, Quantitative X-ray tomography, Int. Mater. Rev. 59 (2014) 1–43.
[25] V. Cnudde, M.N. Boone, High-resolution X-ray computed tomography in geosciences: a review of the current technology and applications, Earth Sci. Rev. 123 (2013) 1–17.
[26] L. Schoeman, P. Williams, A. du Plessis, M. Manley, X-ray micro-computed tomography (μCT) for non-destructive characterization of food microstructure, Trends Food Sci. Technol. 47 (2016) 10–24.
[27] A. du Plessis, S.G. le Roux, A. Guelpa, The CT Scanner Facility at Stellenbosch University: an open access X-ray computed tomography laboratory, Nucl. Inst. Methods Phys. Res. B 384 (2016) 42–49.
[28] I. Vladoiu, M. Stafe, C. Negutu, I.M. Popescu, The dependence of the ablation rate of metals on nanosecond laser fluence and wavelength, J. Optoelectron. Adv. Mater. 10 (2008) 3177–3181.
[29] G. Cristoforetti, S. Legnaioli, V. Palleschi, E. Tognoni, P.A. Benedetti, Observation of different mass removal regimes during the laser ablation of an aluminum target in air, J. Anal. At. Spectrom. 23 (2008) 1518–1528.
[30] B.N. Chichkov, C. Momma, S. Nolte, F. von Alvensleben, A. Tunnermann, Femtosecond, picosecond and nanosecond laser ablation of solids, Appl. Phys. A Mater. Sci. Process. 63 (1996) 109–115.
[31] C. Momma, S. Nolte, N.B. Chichkov, F.V. Alvensleben, A. Tunnermann, Precise laser ablation with ultrashort pulses, Appl. Surf. Sci. 109-110 (1997) 15–19.